

# Flexural behaviors of full-scale prestressed high-performance concrete box girders

Hongye Gou<sup>\*1,2</sup>, Jie Gu<sup>3a</sup>, Zhiwen Ran<sup>1b</sup>, Yi Bao<sup>4c</sup> and Qianhui Pu<sup>1d</sup>

<sup>1</sup>Department of Bridge Engineering, School of Civil Engineering, Southwest Jiaotong University, Chengdu 610031, China

<sup>2</sup>Key Laboratory of High-Speed Railway Engineering, Ministry of Education, Southwest Jiaotong University, Chengdu 610031, China

<sup>3</sup>Graduate School of Tangshan, Southwest Jiaotong University, Tangshan, Hebei 063000, China

<sup>4</sup>Department of Civil, Environmental and Ocean Engineering, Stevens Institute of Technology, Hoboken, NJ 07030, USA

(Received April 13, 2019, Revised March 4, 2020, Accepted March 20, 2020)

**Abstract.** In this study, the flexural behaviors of full-scale prestressed concrete box girders are experimentally investigated. Four girders were fabricated using two types of concrete (compressive strengths: 50 MPa and 70 MPa) and tested under four-point bending until failure. The measured parameters included the deflection, the stress and strain in concrete and steel bars, and cracks in concrete. The measurement results were used to analyze the failure mode, load-bearing capacity, and deformability of each girder. A finite element model is established to simulate the flexural behaviors of the girders. The results show that the use of high-performance concrete and reasonable combination of prestressed tendons could improve the mechanical performance of the box girders, in terms of the crack resistance, load-carrying capacity, stress distribution, and ductility.

**Keywords:** box girder; flexural behavior; full-scale failure test; finite element analysis; high performance concrete

## 1. Introduction

With the rapid development of modern transportation, there are higher requirements for the load-carrying performance and long-term durability of bridges. The use of high-performance construction materials is one of the main ways to improve bridge performance and satisfy the increasing demand (Ning *et al.* 2015, Ehab and Ben 2011). In the current bridge construction practices, most bridges still use concrete with a compressive strength of 40 MPa to 60 MPa (Nie *et al.* 2004, Evangelista *et al.* 2017). Although there are recent studies on high-performance concrete (HPC) and ultra-high-performance concrete (UHPC), there are limited real-life applications in bridge engineering (Qi *et al.* 2019, Liu *et al.* 2019). High-performance concrete commonly refers to concrete whose compressive strength is at least 60 MPa and less than 130 MPa (FIP/CEB 1990). HPC has high compressive strength, excellent durability, high modulus of elasticity, high stiffness, small creep, and economic benefits (Sharifi *et al.* 2014), and provides a solution to reduce sizes and weights of structural components, particularly for long span girders. For the same

girder, if the concrete strength grade is increased from C30 to C60, the mass of concrete can be saved by about 30%-40% for compression members and about 10%-20% for flexural members. The application of HPC also enable structures to be suitable for areas with extreme weather or environment (Djaknoun *et al.* 2010). In order to utilize the capabilities and take full advantages of HPC, there is a trend to adopt HPC in bridges.

The constitutive relationship of HPC has been studied in the literature (Yao *et al.* 2014, Meng *et al.* 2013, Deng *et al.* 2001). Ho *et al.* (2012) studied the advantages and disadvantages of using HPC in concrete beams, and revealed that HPC increased the load-carrying capacity and ductility. Model test and in-situ test are effective to investigate the mechanical performance of bridge structures (Gou *et al.* 2018 a-f). Zheng *et al.* (2012) conducted flexural experiments of 10 simply supported beams made using HPC, studied the failure process, analyzed the failure mechanism, and investigated the influencing factors for the flexural behaviors. Yun *et al.* (2012) tested the load-carrying capacity and ductility of 10 HPC beams through flexural tests, and studied the effects of concrete strength, reinforcement ratio, and shear span to beam depth ratio on ductility. Chiu *et al.* (2018) tested two simple beams and seven cantilever beams, and investigated the flexural crack development of HPC beams.

Currently, there are limited full-scale experiments on prestressed HPC box girders (Weng *et al.* 2002). Compared with reduced-scale models, full-scale models are not subjected to the influences of similarity ratio and size effect on material and structure, and, thus, the test results are more reliable. However, due to difficulties and cost of full-scale models, there are limited experimental data. There is a need to establish a more holistic understanding on the flexural behaviors of prestressed HPC girders through experimental testing and finite element analysis (Gou *et al.* 2019a,b).

\*Corresponding author, Ph.D., Professor

E-mail: [gouhongye@swjtu.edu.cn](mailto:gouhongye@swjtu.edu.cn)

<sup>a</sup> Master student

E-mail: [274765543@qq.com](mailto:274765543@qq.com)

<sup>b</sup> Master student

E-mail: [1770825442@qq.com](mailto:1770825442@qq.com)

<sup>c</sup> Assistant Professor

E-mail: [yi.bao@stevens.edu](mailto:yi.bao@stevens.edu)

<sup>d</sup> Professor

E-mail: [qhpu@vip.163.com](mailto:qhpu@vip.163.com)

Table 1 Details of the tested girders

No.	Concrete type	Type of prestressing	Degree of prestressing
G1	C70	Partially prestressed	1.18
G2	C70	Full prestressed	1.31
G3	C50	Partially prestressed	1.30
G4	C50	Full prestressed	1.17

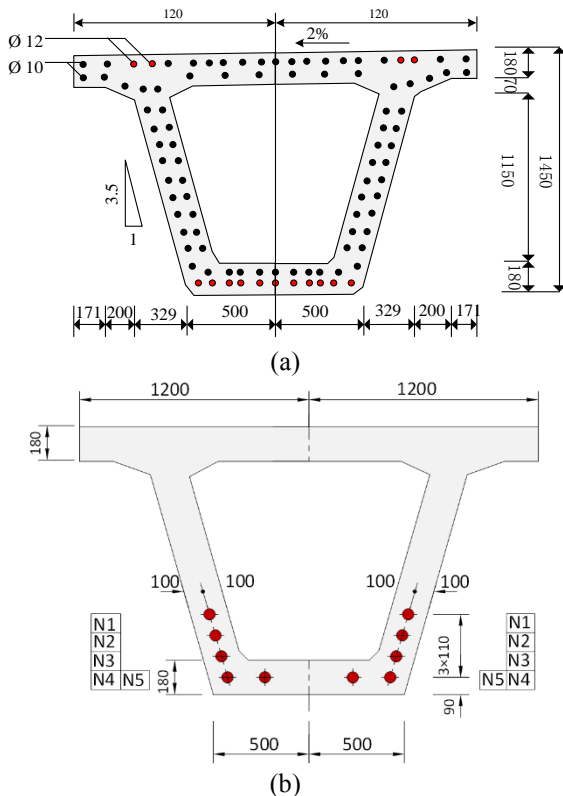


Fig. 1. The mid-span cross section of the box girder (unit: mm): (a) arrangement of steel bars, and (b) arrangement of prestressed tendons.

This study aims to evaluate the flexural behaviors of prestressed concrete box girders through full-scale mode test. To this end, four full-scale girders were fabricated and tested to failure. Two types of concrete were used to fabricate the four girders, and the compressive strengths of the two types of concrete are 50 MPa and 70 MPa, respectively. Throughout the testing, the measurement included the deflection, the stress and strain in concrete and steel bars, and cracks in concrete. The measurement results were used to analyze the failure mode, load-bearing capacity, and deformability of each girder. A finite element model is established to simulate the flexural behaviors of the girders.

## 2. Experiment program

### 2.1 Specimens

Table 1 lists the details of the four box girders, which are designated G1 to G4. Among them, G1 and G2 were made using C70 concrete that has a compressive strength of

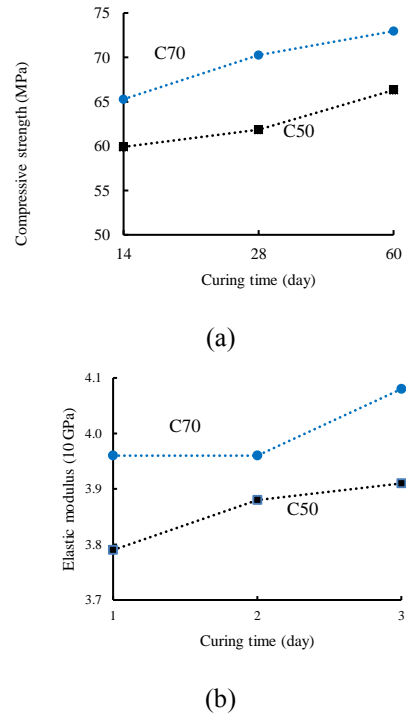


Fig. 2. Concrete properties: (a) compressive strength, and (b) elastic modulus.

70 MPa, while G3 and G4 were made using C50 concrete that has a compressive strength of 50 MPa; G1 and G3 were partially prestressed, while G2 and G4 were fully prestressed. All the girders had the same dimensions and reinforcement. The cross section and arrangement of steel bars and prestressed tendons are shown in Fig. 1.

There were two sizes of longitudinal reinforcing bars, which were 12 mm ( $\Phi 12$ ) and 10 mm ( $\Phi 10$ ) in diameter, respectively, both made of HRB400 steel that has a nominal yielding strength of 400 MPa. The prestressed tendons were 15.2 mm in diameter, and had a nominal tensile strength of 1860 MPa. The control stress was 1395 MPa for the fully prestressed girders and 1245 MPa for the partially prestressed girders.

For each girder, the total span length was 24 m, including two shear spans with a length of 10.5 m at each side and one pure bending length of 3 m in between the two shear spans. The depth of the cross section was 1.4 m, so the shear span to girder depth ratio is 7.5.

## 2.2 Materials

### 2.2.1 Concrete

Concrete specimens were prepared using the same batch of concrete for fabricating the girders, cured under the same condition, and tested to evaluate the mechanical properties. Immediately after concrete casting, the specimens were covered by wet burlap and plastic sheet. The specimens were wetted by spraying water once a day until 3 days after concrete casting, and then, demolded on the 4<sup>th</sup> day. After the specimens were demolded, they were covered by wet burlap and plastic sheet, and kept wet by spraying water every two days until 28 days. Then, the specimens were stored in the laboratory until testing. In the laboratory, the

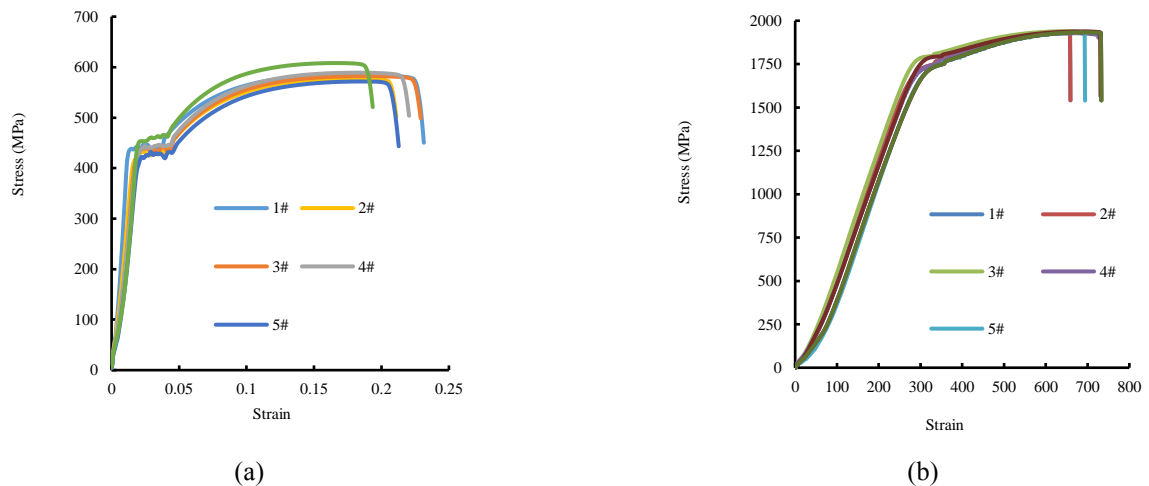


Fig. 3. The tensile stress-strain curves of: (a) steel bars, and (b) prestressed tendons

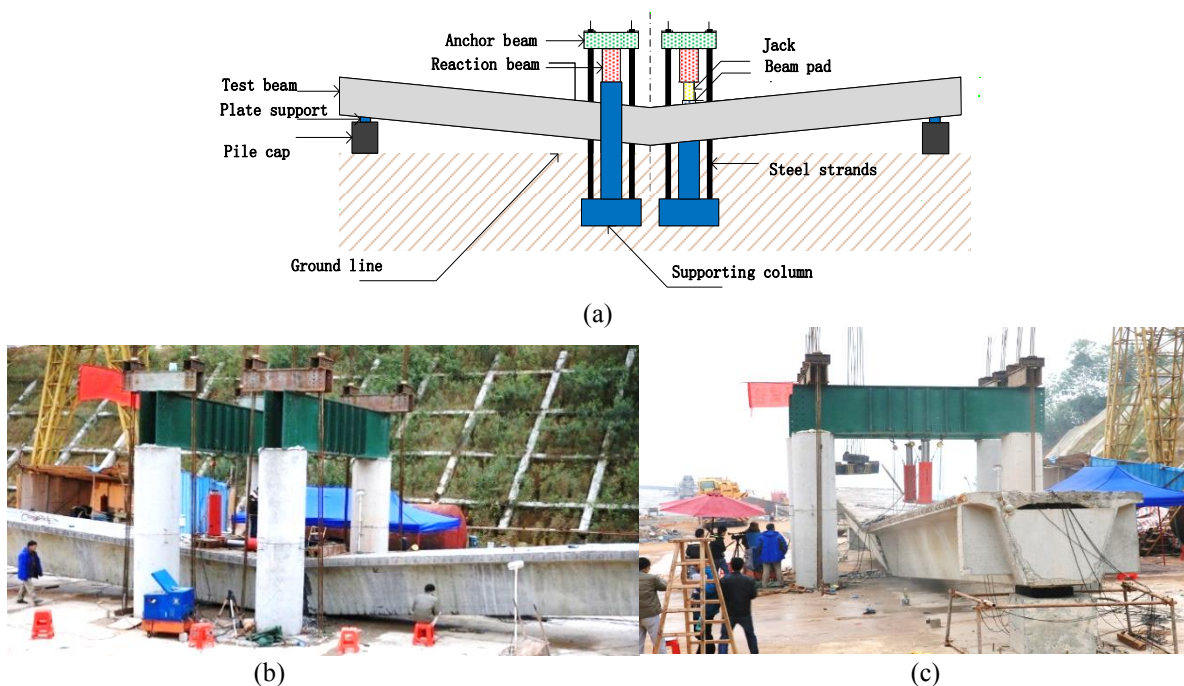


Fig. 4. Test set-up of the full-scale box girders: (a) schematic diagram; (b) front view photo; (c) side view photo.

temperature was sustained at  $20\text{ }^{\circ}\text{C} \pm 2\text{ }^{\circ}\text{C}$  and the relatively humidity was about 50%. The compressive strength and elastic modulus of concrete were tested according to the recommendations in JTG E30 (2005). The compressive strength and elastic modulus were tested using 150 mm cubes. For the elastic modulus, the cube was loaded and unloaded for three cycles. The test results of compressive strength and elastic modulus of concrete are shown in Fig. 2.

### 2.2.2 Steel bars and prestressed tendons

Fig. 3 shows the uniaxial tensile testing results from the steel bars and prestressed tendons. For each testing, five specimens were duplicated. The results from the five specimens were reasonably consistent, indicating that the test results were reliable.

According to the tensile test results of the steel bars, the average yield strength of the steel bars was 432 MPa, the

ultimate strength was 586 MPa, and the Young's modulus was 206 GPa. According to the tensile test results of the prestressed tendons, the average elastic stress limit of the prestressed tendons was 1722 MPa, the average tensile strength was 1935 MPa, and the Young's modulus was 198 GPa. The ductility of the prestressed tendons was much lower than that of the steel bars.

### 2.3 Test setup and loading

Fig. 4 shows the test setup. The girders were tested using a customized reaction frame, which was composed of an anchor girder, a reaction girder, and a support column. Hydraulic jacks were fixed on the reaction frame and used to apply increasing loading until the girder failed. Before the testing, the load-carrying capacity (i.e. the peak load) of each girder was predicted through finite element analysis. A preload of 10% of the peak load was applied to the test girder.

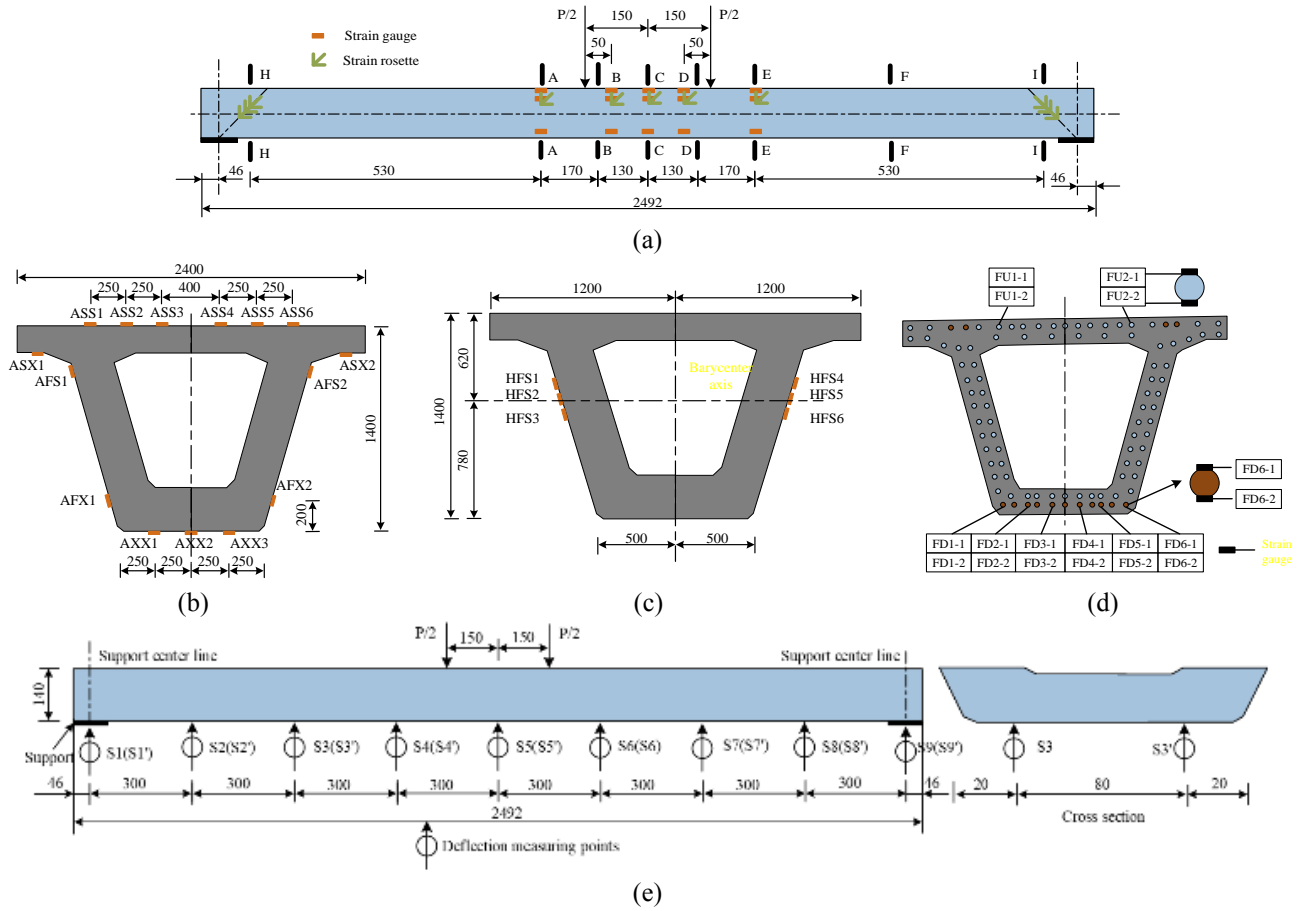


Fig. 5. The measuring points arrangement (unit: mm): (a) front view of arrangement of strain gauges; (b) cross section A; (c) cross sections H and I; (d) Section F; (e) front view of arrangement of displacement sensors

## 2.4 Instrumentation

Fig. 5 shows the arrangement of strain and displacement sensors in the girders. Strain gauges and dial meters were used to measure strain and deformation of each girder, respectively.

The strain gauges were installed at eight cross sections (A, B, C, D, E, F, H, and I) of each girder. Among the eight sections, strain gauges were installed on concrete in seven sections and on steel bars in two sections (C and F). The section F is the quarter span section, and the section C is the mid-span section.

The vertical deflection of each girder was measured using 18 displacement sensors that were equally spaced at 3 m along the girder, as shown in Fig. 5(d).

## 3. Finite element analysis

### 3.1 Concrete constitutive model

Potential damage in concrete is considered in the constitutive model:

$$\sigma = g[D(\varepsilon)]E_c\varepsilon \quad (3-1)$$

where  $g[D(\varepsilon)]$  is the damage variable function (Ding and Yu 2008). The numerical form of the uniaxial stress damage ( $D_0$ ) of concrete is expressed as:

$$D = \begin{cases} \left[ 1 - \left( 1 - \frac{\varepsilon}{\varepsilon_p} \right)^{c_1} \right] D_0, \varepsilon \leq \varepsilon_p \\ 1 - \frac{1 - D_0}{c_2 \left( 1 - D_0 \right) \left( \frac{\varepsilon}{\varepsilon_p} - 1 \right)^{c_3} + 1}, \varepsilon > \varepsilon_p \end{cases} \quad (3-2)$$

Table 2 Parameter expression in damage evolution equation

Uniaxial compression	Uniaxial tension
$D_0 = 2.1 - 0.4 \ln(f_{cu} + 41)$	$D_0 = 0.19$
$c_1 = 0.56 - 0.004 f_{cu}$	$c_1 = 0.31$
$c_2 = 0.17 + 4.34 \times 10^{-5} f_{cu}^{2.8}$	$c_2 = 1.56 + 1.83 \times 10^{-4} f_{cu}^{2.08}$
$c_3 = 0.32 + 0.31 \ln(f_{cu} - 10)$	$c_3 = 1.1 + 3.54 \times 10^{-3} f_{cu}$

where  $\varepsilon$  is the strain of concrete;  $\varepsilon_p$  is the peak strain, and  $\varepsilon_p = 383 f_{cu}^{7/18} \times 10^{-6}$ , where  $f_{cu}$  is the compressive strength.

Table 2 shows the expressions and values of  $D_0$  and parameters ( $c_1$ ,  $c_2$ , and  $c_3$ ), corresponding to the peak strain. According to stress-strain relationship of concrete, the skeleton curve of damage constitutive model of concrete can be obtained. The strain function of concrete under uniaxial compression is:

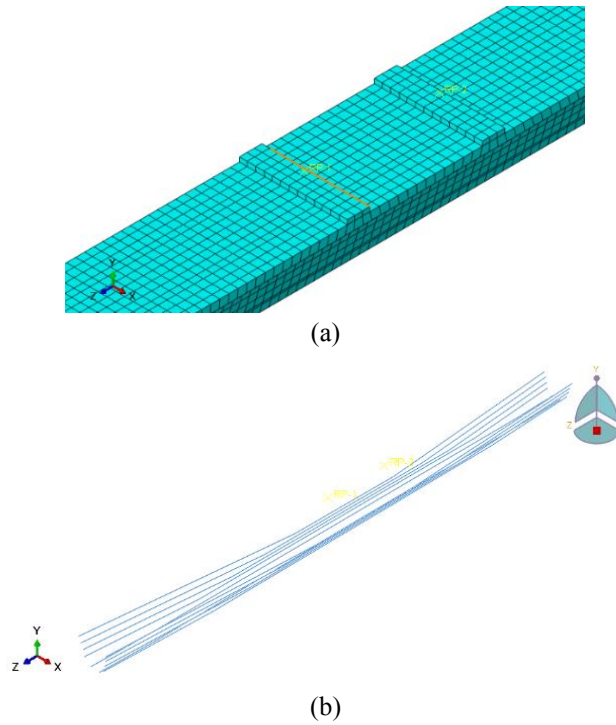


Fig. 6. Finite element model: (a) box girder, and (b) prestressed tendons.

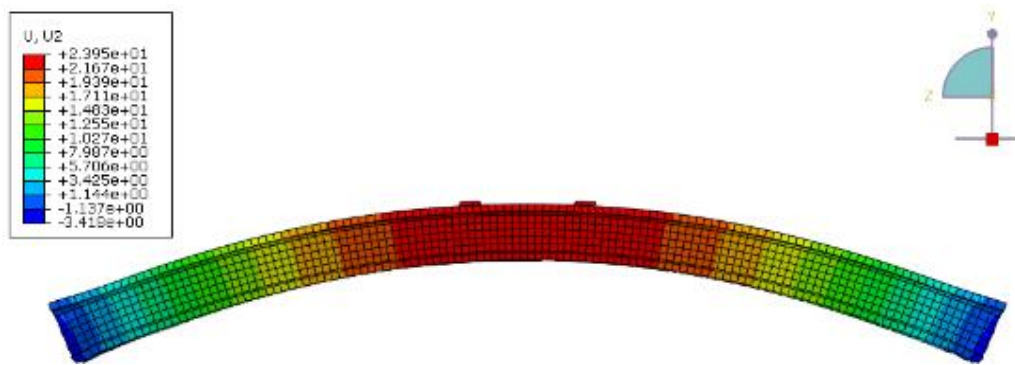


Fig. 7. Camber under prestressing forces.

Table 3 Damage constitutive model of concrete

Stress state	Loading	Unload and reload
Compression	$\sigma = g_c [D_c(\varepsilon)] E_c \varepsilon$	$\sigma = (1 - D_c) E_c (\varepsilon - \varepsilon_0)$
Tension	$\sigma = g_t [D_t(\varepsilon)] E_c \varepsilon$	$\sigma = (1 - D_t) E_c (\varepsilon - \varepsilon_0)$

$$g_c [D_c(\varepsilon)] = \begin{cases} \frac{A_1 - \varepsilon/\varepsilon_c}{A_1 [1 + (A_1 - 2) \varepsilon/\varepsilon_c]} \\ \frac{1}{A_1 [\alpha_1 (\varepsilon/\varepsilon_c - 1)^2 + \varepsilon/\varepsilon_c]} \end{cases} \quad (3-3)$$

where  $A_2 = 1.306$ , and  $\alpha_2 = 1 + 3.4 f_{cu}^2 \times 10^{-4}$ . Besides,  $\varepsilon_t, g_t, D_t$  are the strain, strain function, and damage variable of uniaxial tension, respectively.

The concrete uniaxial damage constitutive model is obtained by combining the above various formulas, and the constitutive relation expression is shown in Table 3.

### 3.2 Finite element model

For each girder, two steel pads are used between the loading point and the girder to distribute the force and avoid stress concentration in the concrete that considers potential damage. The steel pads are attached to the top surface of the flange of the girder.

The concrete and steel pads are simulated using three-dimensional eight-node solid elements (C3D8R); the steel bars and prestressed tendons are simulated using three-dimensional two-node truss elements (T3D2). The truss elements are embedded in the solid elements using the key word “embed”, without considering possible debonding. The paths of the prestressed tendons follow the actual shapes in the girders. Mesh size convergence analysis was conducted, and the global size was determined as 180 mm. The meshed model is shown in Fig. 6.

The prestress in the tendons is applied by applying temperature change:

$$\Delta T = \frac{\sigma}{E\alpha} \quad (3-4)$$

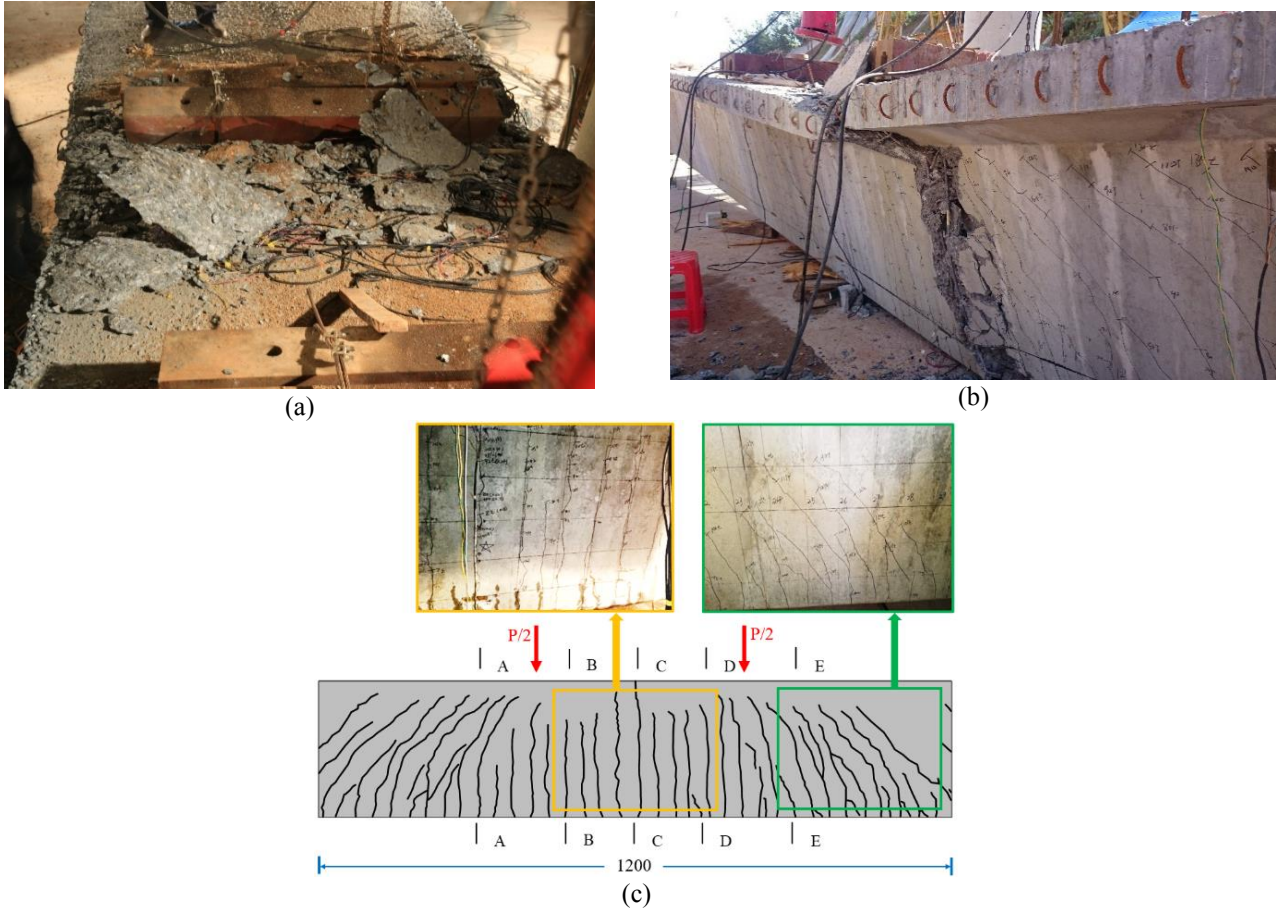


Fig. 8. Photos of G2 after tested to failure: (a) top view of the mid-span section, (b) side view of the mid-span section, and (c) side view of crack pattern.

Table 4 Test and calculation results of camber (mm)

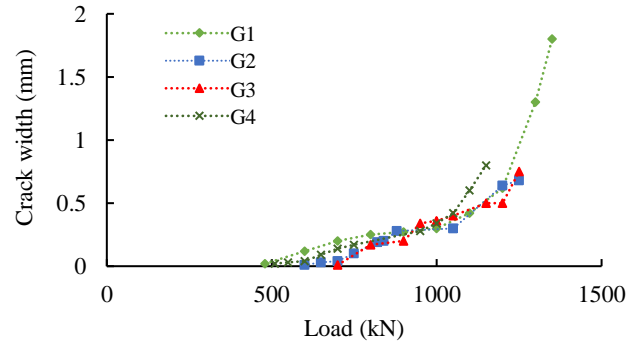
Section No.	L/4		2/L		3L/4	
	Exp	FEA	Exp	FEA	Exp	FEA
G1	17.92	14.12	24.11	20.15	18.09	14.12
G2	20.10	17.15	26.75	23.95	20.00	17.15
G3	19.45	18.24	26.65	25.47	19.85	18.24
G4	15.25	12.45	21.45	21.39	15.80	12.45

where  $\sigma$  is the tensile stress,  $E$  is the Young's modulus of the tendons,  $\alpha$  is the coefficient of expansion ( $\alpha = 10^{-6}$ ). In this study, the stress is 1395 MPa for the fully prestressed girders, and 1246 MPa for the partially prestressed girders.

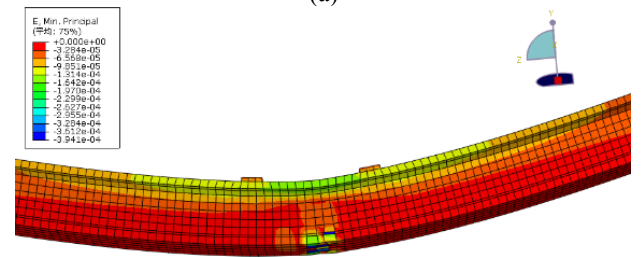
#### 4. Test result and discussion

##### 4.1 Camber

Fig. 7(a) shows the camber of the girder after applying the prestress. The maximum deflection occurs at the mid-span. The experimental and simulation results of camber are compared in Table 4. The experimental results are slightly higher than the simulation results. This is likely due to creeping of concrete, which occurred but is not considered in the finite element analysis.



(a)



(b)

Fig. 9. Development of crack: (a) crack width increases with applied load; (b) cracking initiates at the mid-span under loading.

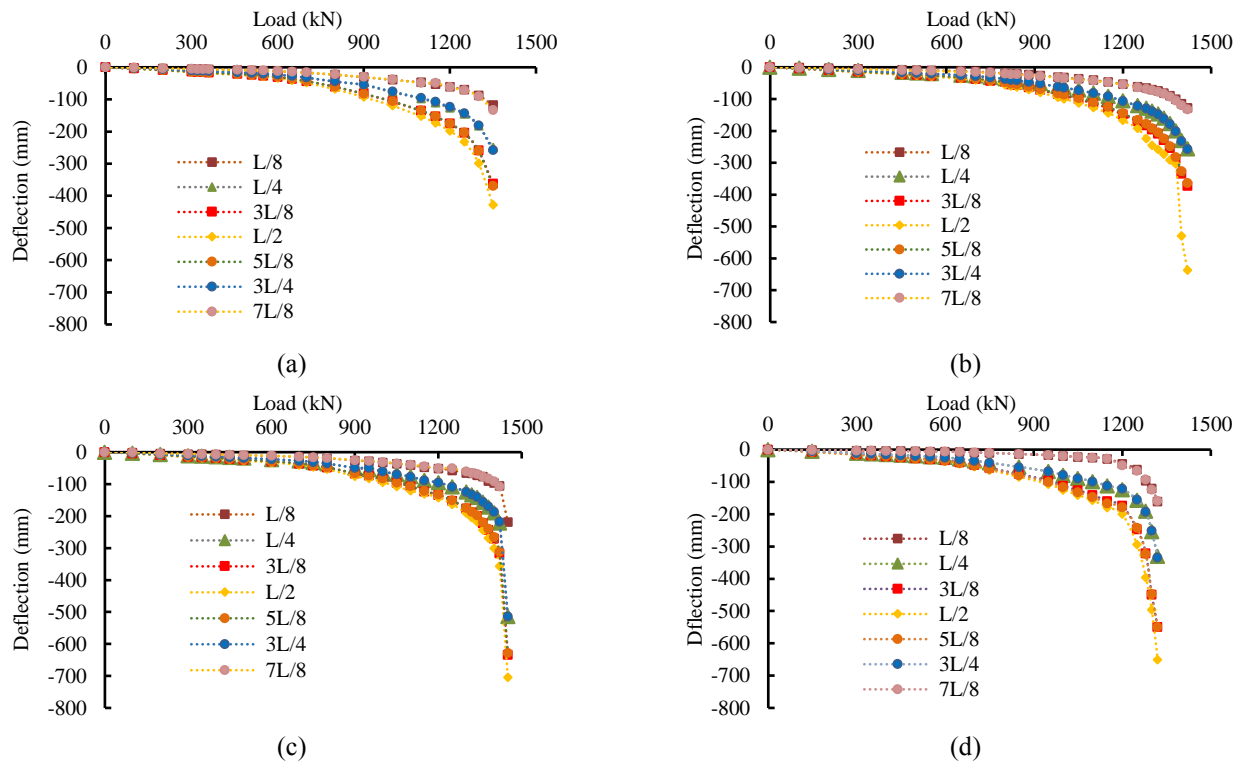


Fig. 10. Load-deflection curves: (a) G1, (b) G2, (c) G3, and (d) G4.

#### 4.2 Failure mode

Fig. 8 depicts the failure mode and crack pattern of G2. As the applied load increased, cracks initiated at the bottom of the girders, because the tensile strain exceeded the cracking strain limit of the concrete.

The cracking load was 580 kN. The first crack appeared at the bottom flange of the section that was about 50 mm away from the mid-span. With further increase of the load, the cracks propagated in the webs and towards the top flange. As the load increased, more cracks were generated, and the crack width increased with the load. Most of the cracks were concentrated within the 12 m length at the mid-span. When the load was increased to 840 kN, the maximum crack width reached 0.2 mm. When the load was increased to 1420 kN, the cracks near the mid-span section were developed into a major crack, chipping of concrete was observed in the top surface of the flange. When the load was increased to 1450 kN, concrete at the top flange near the mid-span was crushed, and the girder could not carry higher load, so the test was terminated. The maximum crack width before the girder failed was 0.68 mm.

The development of the crack width is shown in Fig. 9(a). Under the same load, the crack width of G2 is less than that of G3; the maximum crack width of G2 is 0.68 mm, which is smaller than 0.70 mm of G3. It is speculated that for fully prestressed girders, the use of C70 concrete helps reduce crack width. The maximum crack width of G1 is 1.80 mm, which is larger than that (0.8 mm) of G4, indicating that the crack width of fully prestressed girder is less than that of partially prestressed girder. Fig. 9(b) shows the strain distribution in the girder under cracking load. A crack is generated at the bottom flange of the mid-span section.

Table 5 Experimental and simulation results of stress and strain at the mid-span of girders under cracking load

No.	Strain in mid-span ( $\mu\epsilon$ )		Tension stress (MPa)	
	Exp	FEA	Exp	FEA
G1	105	99.4	4.20	3.99
G2	96	101.6	3.84	4.09
G3	96	101.8	3.84	3.83
G4	97	102.9	3.88	3.86

#### 4.3 Load-deflection curves

Fig. 10 shows the load-deflection curves of the four girders. The four girders follow the same trend of the load-deflection relationship. At the beginning of the loading process, the deflection approximately linearly increases with the applied load, because all materials (i.e. concrete, steel bars, prestressed tendons) behave within their elastic limits. As the load continues increasing, the stresses and strains in materials are increased. As the tensile stress and strain exceed the tensile limits of concrete, cracks are generated in the concrete, as described in section 4.2. Once cracks are generated in concrete, then, stress is redistributed in the cross section with cracks, and the bending stiffness of the girder is decreased due to the presence of cracks. The decrease of bending stiffness is reflected by the change of slope in the load-deflection curves. As the load is further increased, yielding of steel bars is generated, reflected by widening of major cracks and rapid change of slope in the load-deflection curves. Eventually, the girder is failed when the girder cannot resist higher loads, indicated by a zero

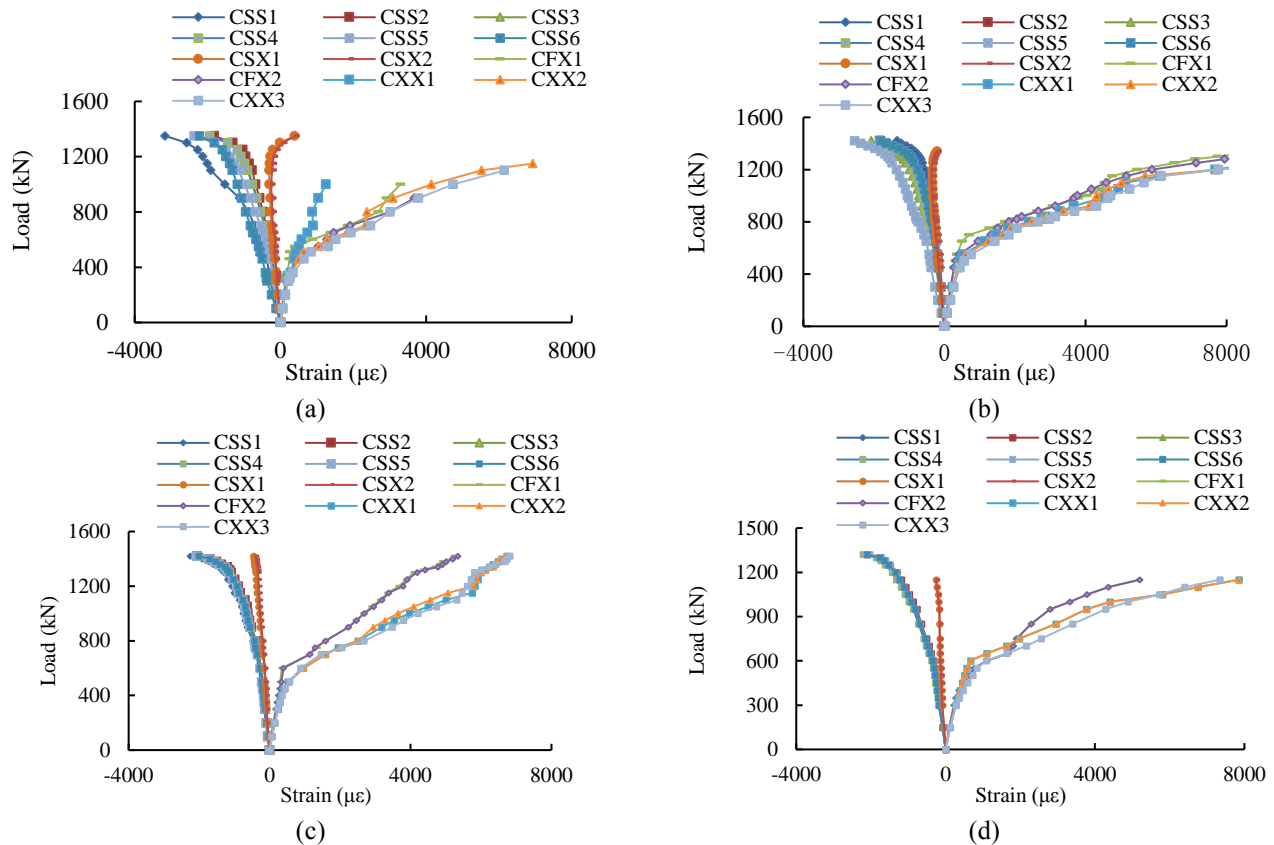


Fig. 11. Load-strain curves of concrete at the mid-span section of: (a) G1, (b) G2, (c) G3, and (d) G4

slope in the load-deflection curves of the tested girders. At the beginning of loading, under the same load, the deflection of G2 is larger than that of G1, and the deflection of G4 is larger than that of G3, indicating that the increase of the degree of prestressing effectively reduces the deflection (Chen and Li 2013).

#### 4.4 Strain

Table 5 lists the experimental and simulation results of the mid-span stress and strain under the cracking load, showing reasonable agreement between each other, thus, indicating that the finite element model can be used to predict the flexural behaviors of the girders.

The load-strain curves of concrete under failure loading is shown in Fig. 11. For G2, when the load is 0~400 kN, the strain approximately linearly increases with the applied load. As the load exceeds 400 kN, the strain increases with a rising rate, because of minor damages in concrete. When the load reaches 580 kN, concrete cracking occurs in the bottom flange. As the load is further increased, more cracks are generated in the concrete until the girder fails. The other three girders show similar trends.

Fig. 12 shows the load-strain curves of longitudinal bars at the mid-span section of girders under failure loads. For G2, when the load is less than 650 kN, the strain approximately linearly increases with the applied load. As the load exceeds 650 kN, the strain increases with a rising rate. When the load reaches 1100 kN, yielding of steel bars occurs. As the load is further increased, more cracks are

generated in the concrete until the girder fails. The other three girders showed similar trends.

When the girders failed, the yielding load of the steel bar is close to the load of concrete crushing, indicating that the failure mode of the girder is reinforced failure. Comparing the load-strain diagrams of four girders, it can be found that the longitudinal reinforcement of some prestressed concrete girders is more regular, the load-strain curve of the steel is smoother, the distortion points are less, the time when the floor bar is unevenly stressed of the fully prestressed concrete girder is earlier than that of partially prestressed concrete girder, which indicate that when the prestressed concrete girder is stressed, the internal stress redistribution of the structure causes the stress in the high stress area to be released to the low area, which better adapts to the stress of the steel bar and maximizes the impact. The material properties of the tensile reinforcement.

## 5. Discussions

### 5.1 Load-carrying capacity

The cracking load of G1 is 480 kN, which is lower than that (580 kN) of G2. From the perspective of crack control, fully prestressed girders show better performance, as shown in Table 6.

Regarding to the ultimate load-carrying capacity, the test results are higher than the simulation results, indicating that the ultimate load of finite element analysis is relatively conservative. Comparing G1 and G2, under prestress, the improvement of load-carrying capacity is insignificant.

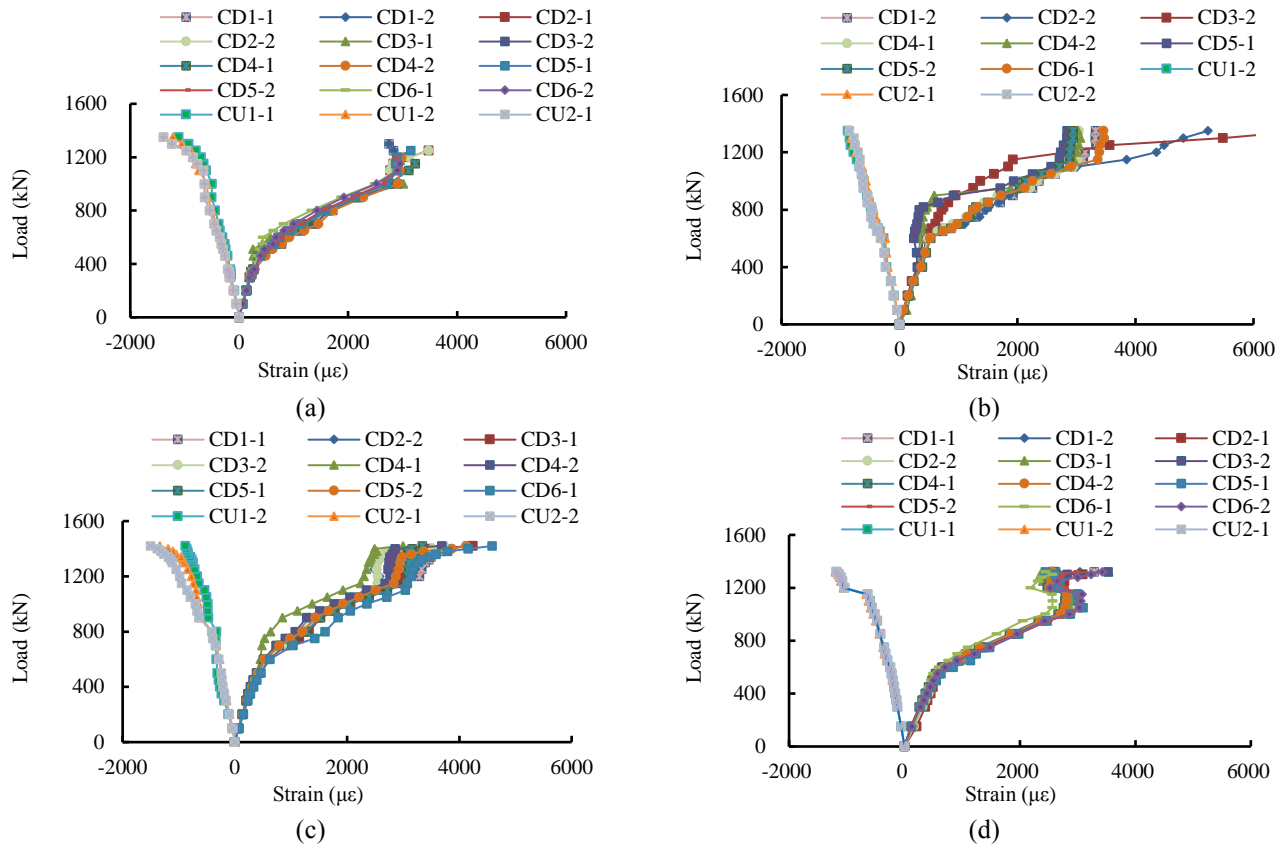


Fig. 12. Load-strain curves of longitudinal steel bars at the mid-span section of: (a) G1, (b) G2, (c) G3, and (d) G4.

Table 6 Comparison of experimental and simulation results

No.	Crack loading		Failure loading	
	Exp	FEA	Exp	FEA
G1	480	480	1350	1237
G2	580	540	1420	1292
G3	550	500	1420	1287
G4	490	450	1320	1232

Comparing G2 and G3, the use of C70 concrete does not improve the load-carrying capacity of the girder. However, the load-carrying capacity of G2 is slightly larger than that of G1, likely because load-carrying capacity of prestressed concrete members controlled by strength and area of steel in tension area. Since the prestress degree of the G2 is larger than G1, the reinforcement ratio of the prestressed steel is larger than G1, the area of the reinforcement is increased, and the load-carrying capacity is increased. As for G2 and G3, when the prestressing degree is the same, the strength and area of the steel in the tension zone are the same, so the load-carrying capacity of the girder is similar.

### 5.2 Ductility

Ductility refers to the ability of a structure or component to withstand deformation without a significant drop in load carrying capacity, and the ability to withstand deformation of the previous section or component that can withstand later deformation. In this paper, displacement ductility

Table 7 Ductility parameter

No.	Yield displacement (mm)	Ultimate displacement (mm)	Displacement ductility ratio
G1	119.7	428.0	3.6
G2	127.0	637.0	5.0
G3	120.5	704.0	5.8
G4	124.4	652.3	5.3

coefficient is introduced to reflect the relative ductility of local ductile structure and the whole ductile component.

The displacement ductility coefficient is defined as the ratio of the maximum displacement to the yield displacement after the member yields:

$$\mu_{\Delta} = \frac{\Delta_u}{\Delta_y} \tag{5-1}$$

where  $\Delta_y$  - the yield displacement of the member;  $\Delta_u$  - the ultimate displacement of the member.

The yield displacement of the girder is considered to be the deflection of the girder from the load increasing linearly to the yield of the steel (Jia et al. 2009). The yield displacement is determined by combining the rate significant change point in the load-deflection curve of Fig. 10 with the steel strain diagram of the girder in Fig. 12. The ultimate displacement is the maximum deflection when the girder is loaded to failure. The displacement ductility coefficient results of each test girder are shown in Table 7.

The displacement ductility coefficient of G3 is 16.6% larger than that of G2, and the ductility coefficient of G4 is

46.6% larger than that of G1, indicating the C70 material reduces the ductility of the girder. This is because C70 concrete has higher Young's modulus than that of C50 concrete. The displacement ductility coefficient of G2 is 40% larger than that of G1, and G3 is 11.2% larger than G4, indicating improvement. The prestressing degree can effectively improve the ductility characteristics of the girder, and the girder body can have a better bearing capacity reserve in the plastic section, and can withstand additional internal forces and deformations generated by factors such as accidental load and temperature change. Regarding the ultimate displacement, that of G2 is 49.9% larger than that of G1, and that of G3 is 8% larger than that of G4, also reflecting that the fully prestressed concrete improves the ductility of the girder.

## 6. Conclusions

Based on the above experimental and numerical studies, the following conclusions can be drawn:

- The use of C70 concrete increased the cracking load and did not significantly increase the load-carrying capacity of the prestressed concrete box girder. The utilize of fully prestressed steel increased both the cracking and ultimate loads. The finite element model could reasonably predict the crack and ultimate loads.
- The use of C70 concrete and partial prestressing improved the stress distribution of the box girder. Internal force was redistributed in the cracked cross section and alleviated stresses in highly stressed area, better adapt to the stress of the steel bar, and maximize the material properties of the tensile reinforcement. It can also effectively delay yielding of steel bars in the tension zone or crushing of concrete in the compression zone.
- The use of C70 concrete improved the maximum deflection of the girder, but it cannot control the lower deflection in the early stage of loading. The use of fully prestressed tendons improved the deflection in the early stage of loading, but did not reduce the ultimate deflection.
- As for ductility, the use of C70 concrete reduces the ductility of the girder. Increasing the degree of prestressing effectively improved the ductility characteristics of the girder, and increased the load-carrying capacity of the girder. From the limit displacement performance, the fully prestressed steel can improve the shape deformation ability of the girder.
- In terms of crack control, the fully prestressed steel can effectively restrain the crack width and control the maximum crack width of the girder body, so that the girder body maintains a good appearance during the stress process. The use of C70 concrete slightly reduced the crack width.

## Acknowledgments

The research was funded by the National Natural Science Foundation of China (Grant No. 51878563), the Sichuan Science and Technology Program (Grant No. 2018JY0294 and 2018JY0549), and the Ministry of Science and Technology of China (Grant No. KY201801005).

## References

- Chen, C. P. and Li, T. Y. (2013), "Experimental Research on Deflection of External Pre-stressed Concrete Beam", *Urban Roads Bridges & Flood Control*, 09, 175-178. (In Chinese)
- Chiu, CK., Chi, KN. and Ho, BT. (2018), "Experimental investigation on flexural crack control for high-strength reinforced-concrete beam members", *Int. J. Concr Struct. M.*, 12: 41, <https://doi.org/10.1186/s40069-018-0253-8>.
- Deng, L. Z., Ghosen, M., Znidaric, A. and Casas, J. R. (2001), "Nonlinear flexural behavior of prestressed concrete girder bridges", *J. Bridge. Eng.*, 6(4), 276.
- Djaknoun, S., Ouedraogo, E. and Benyahia, A. A. (2010), "Fracture toughness of high-performance concrete on three-Point bending notched beams at elevated temperature", *Adv. Mater. Res.*, 89(91), 159-164.
- Ding, F. X., Y, Z. W. and Ou, J. P. (2008), "Damage constitutive model of concrete under uniaxial stress conditions", *J. Chang'an Univ. (Nat. Sci. Edit.)*, 28(04), 70-73. (In Chinese)
- Ehab, E. and Ben, Y. (2011), "Numerical simulation of concrete encased steel composite columns", *J. Constr Steel. Res.*, 67(2), 211-222.
- Evangelista, L. and Brito, J. D. (2017), "Flexural behaviour of reinforced concrete beams made with fine recycled concrete aggregates", *KSCE. J. Civ. Eng.* 21(1), 353-363.
- FIP/CEB (1990). High strength concrete, State of the art report. Bulletin d'Information No. 197, London, UK
- GB-T50107 (2010), Standard for evaluation of concrete compressive strength, Ministry of Housing and Urban-Rural Construction of the People's Republic of China& Ministry of Housing and Urban-Rural Construction of the People's Republic of China, Beijing, China. (in Chinese)
- GB1499.2 (2013), Steel for the reinforcement of concrete-Part2: Hot rolled ribbed bars, General Administration of Quality Supervision, Inspection and Quarantine of the People's Republic of China, Beijing, China. (In Chinese)
- Gou, H. Y., Zhou, W., Chen, G. D., Bao, Y. and Pu, Q. H. (2018a), "In-situ test and dynamic analysis of a double-deck tied-arch bridge", *Steel Compos. Struct.*, 27 (1), 161-175
- Gou, H. Y., Wang, W., Shi, X. Y., Pu, Q. H. and Kang, R. (2018b), "Behavior of steel-concrete composite cable anchorage system", *Steel Compos. Struct.*, 26(1), 115-123.
- Gou, H. Y., Yang, L. C., Leng, D., Bao, Y. and Pu, Q. H. (2018c), "Effect of bridge lateral deformation on track geometry of high-speed railway", *Steel Compos. Struct.*, 29(2), 219-229.
- Gou, H.Y., He, Y.N., Zhou, W., Bao, Y., Chen, G.D. (2018d), "Experimental and numerical investigations of the dynamic responses of an asymmetrical arch railway bridge." *P. I. Mech. Eng. F-J. RAI.*, 232(9): 2309-2323.
- Gou, H. Y., Long, H., Bao, Y., Chen, G. D., Pu, Q. H. and Kang, R. (2018e), "Experimental and numerical studies on stress distributions in girder-arch-pier connections of long-span continuous rigid frame arch railway bridge", *J. Bridge Eng.*, 23 (7), 04018039.
- Gou, H. Y., Shi, X. Y, Zhou, W., Cui, K.\* and Pu, Q. H. (2018f), "Dynamic performance of continuous railway bridges: Numerical analyses and field tests", *P. I. Mech. Eng. F-J. RAI.*, 232(3), 936-955.
- Gou, H.Y., Long, H., Bao, Y., Chen, G.D., Pu, Q.H. (2019a). "Dynamic behavior of hybrid framed arch railway bridge under moving trains." *Struct. Infrastruct Eng.* 15(8): 1015-1024.
- Gou, H.Y., Yang, L.C., Mo Z.X., Guo, W., Shi, X.Y., Bao, Y. (2019b). "Effect of long-term bridge deformations on safe operation of high-speed railway and vibration of vehicle-bridge coupled system." *Int. J. Struct. Stab. Dy.*, 19(9): 1950111.
- Hashemi, S. H, Maghsoudi, A. A. and Rahgozar R. (2009), "Bending response of HSC beams strengthened with FRP

- sheets”, *Sci. Iran.*, **16**(2), 138–14.
- Ho, J. C. M., Lam, J. Y. K. and Kwan, A. K. H. (2012), “Flexural ductility and deformability of concrete beams incorporating high-performance materials”, *The Structural Design of Tall and Special Buildings*, **21**(2), 114-132.
- Jia, J. Q., Yan C. W. and Meng, G. (2009), “Seismic performance of steel reinforced ultra high-strength concrete columns”, *J. Sichuan Univ. (Eng. Sci. Edit.)*, **41**(3), 216-22.
- JTG E30 (2005), Test Method of Cement and Concrete for Highway Engineering, Ministry of Transport of the People's Republic of China, Beijing, China. (In Chinese)
- Meng, G., Zhang, L. H. and Jia, J. Q. (2013), “Numerical analysis on flexural capacity of prestressed steel reinforced ultra-high strength concrete beams”, *Key. Eng. Mater.*, **531**(532), 429-434.
- Nie, J. G., Fan, J. S. and Cai, C. S. (2004), “Stiffness and deflection of steel-concrete composite beams under negative bending”, *ASCE. J. Struct. Eng.*, **130** (11), 1842-1851
- Ning, X. L., Ding, Y. N., Zhang, F. S. and Zhang, Y. L. (2015), “Experimental study and prediction model for flexural behavior of reinforced SCC beam containing steel fibers” , *Constr. Build. Mater.*, **93**, 644-653.
- Qi, J., Bao, Y., Wang, J., Li, L. and Li, W., (2019), “Flexural behavior of an innovative dovetail UHPC joint in composite bridges under negative bending moment”, *Eng. Struct.*, **200**, 109716.
- Liu, Y., Zhang, Q., Meng, W., Bao, Y. and Bu, Y., (2019), “Transverse fatigue behaviour of steel-UHPC composite deck with large-size U-ribs”, *Eng. Struct.*, **180**, 388-399.
- Sharifi, Y. and Maghsoudi, A. A. (2014), “An experimental study on the flexural behavior of heavily steel reinforced beams with high-strength concrete”, *Front. Struct. Civ Eng.*, **8**(1), 46-56.
- Weng, C. C., Yen, S. I. and Jiang, M. H. (2002), “Experimental study on shear splitting failure of full-scale composite concrete encased steel beam”, *ASCE. J. Struct. Eng.*, **128**(9), 1186-1194.
- Yan, C. W., Jia, J. Q. and Zhang, J. (2010), “Seismic behavior of steel reinforced ultra high strength concrete column and reinforced concrete beam connection”, *Trans. Tianjin Univ.*, **16**(4), 309-316.
- Yao, Y. D., Wu, F. and Yu, F. (2014), “Shear performance of prestressed ultra high strength concrete encased steel beams”, *Constr. Build. Mater.*, **52**, 194-201.
- Yu, F., Yao D. L., Jia J. Q. and Wu, F. (2014), “Shear behavior of a novel prestressed concrete beam subjected to monotonic and cyclic loading”, *Tran. Tianjin. Univ.*, **20**(3), 75-86.
- Yun, Y. W., Luo, Q., Jang, I. Y., Sun, S. S. and Zhang, J. W. (2012), “Experimental Research on the Ductility of High Performance Concrete Beams”, *Appl. Mech. Mater.*, **166**(169), 1316-1320.
- Zheng, S. S., Zhu, S. S., Hou, P. J., and Che, S. L. (2012), “Experimental Study on the Flexural Behavior of SRHSHPC Beam”, *Appl. Mech. Mater.*, **166**(169), 1502-1505.